

Bhabha scattering in the gauge-Higgs unification

Shuichiro Funatsu¹, Hisaki Hatanaka², Yutaka Hosotani³, Yuta Orikasa⁴ and
Naoki Yamatsu⁵

¹*Institute for Promotion of Higher Education, Kobe University, Kobe 657-0011, Japan*

²*Osaka, Osaka 536-0014, Japan*

³*Department of Physics, Osaka University, Toyonaka, Osaka 560-0043, Japan*

⁴*Institute of Experimental and Applied Physics, Czech Technical University in Prague,
Husova 240/5, 110 00 Prague 1, Czech Republic*

⁵*Department of Physics, Kyushu University, Fukuoka 819-0395, Japan*

Abstract

We examine effects of Z' bosons in gauge-Higgs unification (GHU) models at $e^+e^- \rightarrow e^+e^-$ Bhabha scatterings. We evaluate differential cross sections in Bhabha scatterings including Z' bosons in two types of $SO(5) \times U(1) \times SU(3)$ GHU models. We find that deviations of differential cross sections in the GHU models from those in the SM can be seen at $\sqrt{s} = 250$ GeV. With 80 %-longitudinally polarized electron and 30 %-longitudinally polarized positron beams, the left-right asymmetries in the GHU A- and B-models are resolved at more than 3σ at $L_{\text{int}} = 250 \text{ fb}^{-1}$. We also show that Bhabha scattering with scattering angle less than 100 mrad can be safely used as luminosity measurements at e^+e^- colliders since the effects of Z' bosons are well suppressed for small scattering angle. We propose a new observable which can be measured at future TeV-scale e^+e^- linear colliders.

1 Introduction

With the establishment of the standard model (SM) by the discovery of the Higgs boson, searching for physics beyond the SM (BSM) and understanding the electroweak phase transition have become main topics in particle physics. As one scenario of BSM, the gauge-Higgs unification (GHU) scenario has been studied [1–15]. In GHU, the Higgs boson is a part of the extra-dimensional component of gauge potentials, appearing as a fluctuation mode of an Aharonov-Bohm (AB) phase θ_H in the fifth dimension. Many GHU models are proposed for electroweak unification [16–35], and GHU models for grand unification are also proposed [36–45]. Among them, two types of $SU(3)_C \times SO(5) \times U(1)_X$ GHU models, the A-model [16–22] and B-model [23–28], in warped spacetime have been extensively studied. At low energies below the electroweak scale the mass spectrum and gauge and Higgs couplings of SM particles are nearly the same as in the SM.

Couplings of the first Kaluza-Klein (KK) neutral gauge bosons to right-handed SM fermions are large in the A-model, whereas those to left-handed SM fermions become large in the B-model. In proton-proton collisions KK bosons of photons and Z bosons appear as huge broad resonances of Z' bosons in the Drell-Yan process, and can be seen in current and future hadron collider experiments [19, 20, 28]. The KK-excited states of the W boson are also seen as resonances of W' bosons. In the A-model the couplings of the first KK W boson to the SM fermions are small. In the B-model the couplings of the first KK W boson to right-handed fermions are negligible, while the couplings to left-handed fermions are much larger than the W boson couplings. Therefore at the LHC the first KK W boson appears as a narrow resonance of W' boson in the A-model, but appears as a broad resonance in the B-model [20, 28].

In e^+e^- collider experiments, effects of GHU can be examined by exploring interference effects among photon, Z boson and Z' bosons. In the previous papers we have studied effects of new physics (NP) on such observable quantities as cross section, forward-backward asymmetry and left-right asymmetry in $e^+e^- \rightarrow f\bar{f}$ ($f \neq e$) with polarized and unpolarized e^+e^- beams [21, 25, 30, 31, 49–51]. In Ref. [21] we compared such observable quantities of GHU with those of the SM in LEP experiments at $\sqrt{s} = M_Z$, and LEP2 experiments for $130\text{GeV} \leq \sqrt{s} \leq 207\text{GeV}$ [52, 53]. In Refs. [21, 25] we also gave predictions of several signals of Z' bosons in GHU in e^+e^- collider experiments designed for future with collision energies $\sqrt{s} \geq 250\text{GeV}$ with polarized electron and positron beams. In the $e^+e^- \rightarrow f\bar{f}$ ($f \neq e$) modes, the deviations of total cross sections become large for

right-polarized electrons in the A-model, whereas in the B-model the deviations are large for left-polarized electrons.

Deviations from the SM can be seen in the Higgs couplings as well. HWW , HZZ and Yukawa couplings deviate from those in the SM in a universal manner [16, 17, 32]. They are suppressed by a common factor

$$\frac{g_{HWW}^{\text{GHU}}}{g_{HWW}^{\text{SM}}}, \frac{g_{HZZ}^{\text{GHU}}}{g_{HZZ}^{\text{SM}}} \simeq \cos(\theta_H) \quad (1)$$

for W and Z bosons, and

$$\frac{y_{ff}^{\text{GHU}}}{y_{ff}^{\text{SM}}} \simeq \begin{cases} \cos(\theta_H) & \text{A-model [17]} \\ \cos^2(\theta_H/2) & \text{B-model [24]} \end{cases} \quad (2)$$

for SM fermions f . In the analysis of both Z' and W' bosons in hadron colliders [19, 20, 28], it is found that the AB phase is constrained as $\theta_H \lesssim 0.1$. For $\theta_H = \mathcal{O}(0.1)$, probable values in the model, the deviation of the couplings amounts to $(1 - \cos \theta_H) = \mathcal{O}(0.005)$, and is small. At the International Linear Collider (ILC) at $\sqrt{s} = 250\text{GeV}$, the ZZH coupling can be measured in the 0.6 % accuracy with 2 ab^{-1} data [47]. Since the masses and Higgs couplings of the SM fields in the GHU models are very close to those in the SM, the electroweak phase transition (EWPT) occurs at $T_C \sim 160\text{GeV}$ and appears very weak first order [22, 27] in both A- and B-models, which is very similar to EWPT in the SM [48].

In this paper we study effects of Z' bosons in GHU models on the $e^+e^- \rightarrow e^+e^-$ Bhabha scattering. Measurements of Bhabha scattering at linear colliders have contributed to the establishment of the SM [56–58]. Bhabha scattering is also useful to explore NP [59, 60]. Unlike $e^+e^- \rightarrow f\bar{f}$ ($f \neq e$) scattering, in Bhabha scattering not only s -channel but also t -channel contributions enter the process. Since the t -channel contribution of photon exchange dominates in forward scattering amplitudes, the cross section becomes very large for small scattering angles, which improves the statistics of experiments. It will be seen below that effects of Z' bosons on cross sections can be measured with large significances.

Bhabha scattering at very small scattering angles is used for the determination of the luminosity of the e^+e^- beams. Since cross sections of all other scattering processes depend on the luminosity, one needs to know whether or not effects of Z' bosons on the $e^+e^- \rightarrow e^+e^-$ cross section are sufficiently small. Forward-backward asymmetry A_{FB} of the cross section in Bhabha scattering is no longer a good quantity for searching NP, since the backward scattering cross section is much smaller than the forward scattering

cross section. We will propose a new quantity A_X to measure with polarized e^+e^- beams, which can be used for seeing NP effects instead of A_{FB} .

In Section 2 we briefly review the GHU A- and B-models and discuss the $e^+e^- \rightarrow e^+e^-$ scattering in both the SM and GHU models. In Section 3, we show the formulas of $e^+e^- \rightarrow e^+e^-$ scattering cross sections for longitudinally polarized e^\pm beams, and numerically evaluate the effects of Z' bosons in GHU models on differential cross sections and left-right asymmetries. We also show that effects of Z' bosons on the cross section are very small at the very small scattering angle.

2 Gauge-Higgs unification

In GHU A- and B-models the electroweak $SU(2) \times U(1)$ symmetry is embedded in $SO(5) \times U(1)_X$ symmetry in the Randall-Sundrum warped space [46], whose metric is given by

$$ds^2 = \frac{1}{z^2} \left[\eta_{\mu\nu} dx^\mu dx^\nu + \frac{dz^2}{k^2} \right], \quad 1 \leq z \leq z_L = e^{kL} \quad (3)$$

where $\eta_{\mu\nu} = \text{diag}(-1, +1, +1, +1)$ and k is the AdS-curvature. We refer two 4D hyperplanes at $z = 1$ and $z = z_L$ as the UV and IR branes, respectively. The $SO(5)$ symmetry is broken to $SO(4) \simeq SU(2)_L \times SU(2)_R$ by the boundary conditions at $z = 1, z_L$ and the $SU(2)_R \times U(1)_X$ symmetry is broken to $U(1)_Y$ by a scalar field localized on the UV brane. $SU(2)_L \times U(1)_Y$ symmetry is broken to the electromagnetic $U(1)_{\text{EM}}$ symmetry by the VEV of the z -component gauge fields of $SO(5)/SO(4)$. The VEV is related to the gauge-invariant AB phase θ_H .

The difference between the A- and B-models lies in the content of fermions as tabulated in Table 1. In the A-model, quarks and leptons in the SM are embedded in the $SO(5)$ -vector representation. In the B-model quarks and leptons are embedded in the $SO(5)$ -spinor, vector and singlet representations, which are naturally derived from spinor and vector multiplets in the $SO(11)$ gauge-Higgs grand unification [37, 38]. We also note that the bulk mass parameter for the bulk electron field, c_e , is positive in the A-model [18] whereas c_e in the B-model has to be negative [23]. In the B-model positive c_e leads to an exotic light neutrino state and therefore negative c_e must be chosen. Zero modes of fermion fields with positive bulk mass parameters are localized near the UV brane whereas zero modes of fermion fields with negative bulk mass parameters are localized near the IR brane.

Table 1: The fermion content in the first generation of the lepton sector is shown. In the A-model bulk fermions are introduced in the vector representation of $SO(5)$, which are decomposed of $SO(4)$ -vector and singlet. Zero modes of fermions appear in the left-handed components of $SO(4)$ -vectors and in the right-handed components of $SO(4)$ -singlets. The extra zero modes of L_j ($j = 1, 2, 3$) couple to brane fermions at the UV brane to become massive [18]. In the B-model bulk fermions are introduced in the spinor representation of $SO(5)$. Zero modes appear in the left-handed components of $SU(2)_L$ doublet (ν_e, e) and in the right-handed components of $SU(2)_R$ doublet (ν'_e, e') [23].

	A-model	B-model
Bulk fermion	$\left(\begin{pmatrix} \nu_e & L_{1X} \\ e & L_{1Y} \end{pmatrix}, e' \right), \left(\begin{pmatrix} L_{2X} & L_{3X} \\ L_{2Y} & L_{3Y} \end{pmatrix}, \nu'_e \right)$	$\begin{pmatrix} \nu_e \\ e \\ \nu'_e \\ e' \end{pmatrix}$

Interactions of the electron and gauge bosons are given by

$$\int d^4x \int_1^{z_L} \frac{dz}{k} \left\{ \bar{\Psi} \gamma^\mu (\partial_\mu - ig A_\mu) \Psi \right\} \quad (4)$$

where $A_\mu(x, z)$ is a four-dimensional component of the 5D gauge field and $\Psi(x, z) = z^2 \check{\Psi}$ is the 5D electron field. The electron corresponds to the zero mode of $\check{\Psi}(x, z)$. In the A-model the left-handed electron is localized in the vicinity of the UV brane and the right-handed component is localized near the IR brane. In the B-model the right-handed electron is localized in the vicinity of the UV brane and the left-handed component is localized near the IR brane. $A_\mu(x, z)$ has a KK expansion which contains the photon, Z boson and their KK excited modes. The wave function of the photon is constant in the fifth dimension coordinate z . The wave function of the Z boson is almost constant in z , but has nontrivial dependence near the IR brane. Couplings of the electron to the Z boson are very close to those in the SM. Wave functions of the first KK-excited modes of gauge bosons are localized near the IR brane so that the first KK-excited gauge bosons couple strongly with fermions localized near the IR brane. In the A-model right-handed electrons have large couplings to the first KK-excited gauge bosons whereas in the B-model left-handed electrons couple strongly to the first KK-excited gauge bosons.

Table 2: Parameters in GHU models. c_e in the rightest column is the bulk parameter for the electron field.

Model	θ_H [rad]	m_{KK} [TeV]	z_L	$m_{\gamma^{(1)}}$ [TeV]	$\Gamma_{\gamma^{(1)}}$ [TeV]	$m_{Z^{(1)}}$ [TeV]	$\Gamma_{Z^{(1)}}$ [TeV]	$m_{Z_R^{(1)}}$ [TeV]	$\Gamma_{Z_R^{(1)}}$ [TeV]	c_e
A	0.08	9.54	1.01×10^4	7.86	0.99	7.86	0.53	7.31	1.01	2.0342
B	0.10	13.0	3.87×10^{11}	10.2	3.25	10.2	7.84	9.95	0.816	-1.0067

Table 3: Left-handed and right-handed couplings of the electron, ℓ_V, r_V ($V = Z, Z^{(1)}, Z_R^{(1)}$ and $\gamma^{(1)}$), in units of $g_w \equiv g_A/\sqrt{L}$ (see text). Ratios of e and g_w are shown in the second column.

Model	$(e/g_w)^2$	ℓ_Z	r_Z	$\ell_{Z^{(1)}}$	$r_{Z^{(1)}}$	$\ell_{Z_R^{(1)}}$	$r_{Z_R^{(1)}}$	$\ell_{\gamma^{(1)}}$	$r_{\gamma^{(1)}}$
A	0.2312	-0.3066	0.2638	0.1195	0.9986	0.0000	-1.3762	0.1879	-1.8171
B	0.2306	-0.3058	0.2629	-1.7621	-0.0584	-1.0444	0.0000	-2.7587	0.1071

In Tables 2 and 3, parameters and couplings in the A- and B-models are tabulated. Here, model parameters (θ_H, m_{KK} and z_L), masses, widths and couplings of Z' -bosons are referred from Refs. [25, 26]. The big difference in the magnitude of z_L in the A- and B-models originates from the formulas of top-quark mass. In the A-model $m_{\text{top}}^A \simeq (m_{KK}/(\sqrt{2}\pi))\sqrt{1 - 4c_{\text{top}}^2} \sin \theta_H$ [18] whereas in the B-model $m_{\text{top}}^B \simeq (m_{KK}/\pi)\sqrt{1 - 4c_{\text{top}}^2} \sin \frac{1}{2}\theta_H$ [23]. In both models the W boson mass is given by $m_W \simeq m_{KK}/(\pi\sqrt{kL}) \sin \theta_H$ so that the lower bound of z_L becomes $z_L \gtrsim 8 \times 10^3$ in the A-model and $z_L \gtrsim 7 \times 10^7$ in the B-model. In Table 2 the bulk mass parameter for the electron field c_e is given. As explained before, c_e is positive in the A-model whereas c_e is negative in the B-model. In Table 3, the left- and right-handed electron couplings to Z' bosons, r_V, ℓ_V ($V = Z, Z^{(1)}, Z_R^{(1)}, \gamma^{(1)}$), are tabulated. In the table $g_w \equiv g_A/\sqrt{L}$ is the 4D gauge coupling of the SO(5) where g_A is the 5D SO(5) coupling. In terms of g_A and the 5D U(1)_X coupling g_B , a mixing parameter is defined as [19, 25]

$$e/g_w = \sin \theta_W^0 \equiv \frac{s_\phi}{\sqrt{1 + s_\phi^2}}, \quad s_\phi \equiv g_B/\sqrt{g_A^2 + g_B^2}. \quad (5)$$

The value of $\sin \theta_W^0$ is determined so as to reproduce the experimental value of the forward-backward asymmetry in $e^+e^- \rightarrow \mu^+\mu^-$ scattering at the Z -pole. In the A-model electron's right-handed couplings to Z' -bosons are larger than left-handed couplings. In the B-model electron's left-handed couplings to Z' -bosons are larger than right-handed couplings.

3 Bhabha scattering in e^+e^- colliders

We consider the $e^+e^- \rightarrow e^+e^-$ scattering in the center-of-mass frame. In this frame, the Mandelstam variables (s, t, u) are given by

$$\begin{aligned} s &= 4E^2, \\ t &= -\frac{s}{2}(1 - \cos \theta) = -s \sin^2 \frac{\theta}{2}, \\ u &= -\frac{s}{2}(1 + \cos \theta) = -s \cos^2 \frac{\theta}{2} \end{aligned} \quad (6)$$

where E is the energy of initial electron and positron, and θ is the scattering angle of the electron. Since the $e^+e^- \rightarrow e^+e^-$ scattering process consists both s - and t -channel processes, the scattering amplitude is written in terms of the following six building blocks:

$$\begin{aligned} S_{LL} &= S_{LL}(s) \equiv \sum_i \frac{\ell_{V_i}^2}{s - M_{V_i}^2 + iM_{V_i}\Gamma_{V_i}}, \\ S_{RR} &= S_{RR}(s) \equiv \sum_i \frac{r_{V_i}^2}{s - M_{V_i}^2 + iM_{V_i}\Gamma_{V_i}}, \\ S_{LR} &= S_{LR}(s) \equiv \sum_i \frac{\ell_{V_i} r_{V_i}}{s - M_{V_i}^2 + iM_{V_i}\Gamma_{V_i}}, \\ T_{LL} &= T_{LL}(s, \theta) \equiv \sum_i \frac{\ell_{V_i}^2}{t - M_{V_i}^2 + iM_{V_i}\Gamma_{V_i}}, \\ T_{RR} &= T_{RR}(s, \theta) \equiv \sum_i \frac{r_{V_i}^2}{t - M_{V_i}^2 + iM_{V_i}\Gamma_{V_i}}, \\ T_{LR} &= T_{LR}(s, \theta) \equiv \sum_i \frac{\ell_{V_i} r_{V_i}}{t - M_{V_i}^2 + iM_{V_i}\Gamma_{V_i}}, \end{aligned} \quad (7)$$

where M_{V_i} and Γ_{V_i} are the mass and width of the vector boson V_i . ℓ_{V_i} and r_{V_i} are left- and right-handed couplings of electrons to the vector boson V_i ($V_0 = \gamma$, $V_1 = Z$), respectively. In particular, we have $\ell_\gamma = r_\gamma = Q_e e$, $Q_e = -1$, $\ell_Z = \frac{e}{\sin \theta_W^0 \cos \theta_W^0} [I_e^3 - Q_e \sin^2 \theta_W^0]$, $r_Z = \frac{e}{\sin \theta_W^0 \cos \theta_W^0} [-Q_e \sin^2 \theta_W^0]$, $I_e^3 = -\frac{1}{2}$ in the SM. Here e , I_e^3 and θ_W^0 are the electromagnetic coupling, weak isospin of the electron and the bare Weinberg angle defined in (5), respectively.

When initial state electrons and positrons are longitudinally polarized, the differential cross section is given by

$$\begin{aligned} \frac{d\sigma}{d\cos \theta}(P_{e^-}, P_{e^+}) &= \frac{1}{4} \left\{ (1 + P_{e^-})(1 + P_{e^+}) \frac{d\sigma_{e_R^- e_R^+}}{d\cos \theta} + (1 - P_{e^-})(1 - P_{e^+}) \frac{d\sigma_{e_L^- e_L^+}}{d\cos \theta} \right. \\ &\quad \left. + (1 + P_{e^-})(1 - P_{e^+}) \frac{d\sigma_{e_R^- e_L^+}}{d\cos \theta} + (1 - P_{e^-})(1 + P_{e^+}) \frac{d\sigma_{e_L^- e_R^+}}{d\cos \theta} \right\}, \end{aligned} \quad (8)$$

where P_{e^-} and P_{e^+} are the polarization of the electron and positron beam, respectively. $P_{e^-} = +1$ ($P_{e^+} = +1$) denotes purely right-handed electrons (positrons) [54, 55]. $\sigma_{e_X^- e_Y^+}$ ($X, Y = L, R$) denotes the cross section for left-handed or right-handed electron and positron. When the electron mass is neglected, these cross sections are given by

$$\begin{aligned}\frac{d\sigma_{e_L^- e_R^+}}{d\cos\theta} &= \frac{1}{8\pi s} (u^2 |S_{LL} + T_{LL}|^2 + t^2 |S_{LR}|^2), \\ \frac{d\sigma_{e_R^- e_L^+}}{d\cos\theta} &= \frac{1}{8\pi s} (u^2 |S_{RR} + T_{RR}|^2 + t^2 |S_{LR}|^2), \\ \frac{d\sigma_{e_L^- e_L^+}}{d\cos\theta} &= \frac{d\sigma_{e_R^- e_R^+}}{d\cos\theta} = \frac{1}{8\pi s} \cdot (s^2 |T_{LR}|^2).\end{aligned}\quad (9)$$

When $s, t \ll M_Z^2$, the cross section is approximated by the one at the QED level, where we obtain $S_{LL} = S_{RR} = S_{LR} = e^2/s$ and $T_{LL} = T_{RR} = T_{LR} = e^2/t$, and

$$\frac{d\sigma_{\text{QED}}}{d\cos\theta}(P_{e^-}, P_{e^+}) = \frac{e^4}{16\pi s} \left\{ (1 - P_{e^-} P_{e^+}) \frac{t^4 + u^4}{s^2 t^2} + (1 + P_{e^-} P_{e^+}) \frac{s^2}{t^2} \right\}. \quad (10)$$

For unpolarized electron or positron beams, the above expression reduces to a familiar formula

$$\frac{d\sigma_{\text{QED}}^{\text{unpolarized}}}{d\cos\theta} = \frac{e^4}{16\pi s} \frac{s^4 + t^4 + u^4}{s^2 t^2}. \quad (11)$$

We also note that in terms of building blocks (7) we can write down components of s-, t-channels, and interference terms as

$$\frac{d\sigma}{d\cos\theta} = \frac{d\sigma^{\text{s-channel}}}{d\cos\theta} + \frac{d\sigma^{\text{t-channel}}}{d\cos\theta} + \frac{d\sigma^{\text{interference}}}{d\cos\theta}, \quad (12)$$

where each component is given by

$$\begin{aligned}\frac{d\sigma^{\text{s-channel}}}{d\cos\theta}(P_{e^-}, P_{e^+}) &= \frac{1}{32\pi s} \left\{ (1 + P_{e^-})(1 - P_{e^+}) [u^2 |S_{RR}|^2 + t^2 |S_{LR}|^2] \right. \\ &\quad \left. + (1 - P_{e^-})(1 + P_{e^+}) [u^2 |S_{LL}|^2 + t^2 |S_{LR}|^2] \right\}, \\ \frac{d\sigma^{\text{t-channel}}}{d\cos\theta}(P_{e^-}, P_{e^+}) &= \frac{1}{32\pi s} \left\{ (1 + P_{e^-})(1 + P_{e^+}) s^2 |T_{LR}|^2 + (1 - P_{e^-})(1 - P_{e^+}) s^2 |T_{LR}|^2 \right. \\ &\quad \left. + (1 + P_{e^-})(1 - P_{e^+}) u^2 |T_{RR}|^2 + (1 - P_{e^-})(1 + P_{e^+}) u^2 |T_{LL}|^2 \right\}, \\ \frac{d\sigma^{\text{interference}}}{d\cos\theta}(P_{e^-}, P_{e^+}) &= \frac{1}{16\pi s} u^2 \left\{ (1 + P_{e^-})(1 - P_{e^+}) \text{Re}(S_{RR} T_{RR}^*) \right. \\ &\quad \left. + (1 - P_{e^-})(1 + P_{e^+}) \text{Re}(S_{LL} T_{LL}^*) \right\}.\end{aligned}\quad (13)$$

When initial electrons and/or positrons are longitudinally polarized, one can measure left-right asymmetries. The left-right asymmetry of polarized cross sections is given by

$$\begin{aligned}
A_{LR}(P_-, P_+) &\equiv \frac{\sigma(P_{e^-} = -P_-, P_{e^+} = -P_+) - \sigma(P_{e^-} = +P_-, P_{e^+} = +P_+)}{\sigma(P_{e^-} = -P_-, P_{e^+} = -P_+) + \sigma(P_{e^-} = +P_-, P_{e^+} = +P_+)} \\
&= (P_- - P_+) \cdot \frac{\sigma_{e_L^- e_R^+} - \sigma_{e_R^- e_L^+}}{(1 + P_- P_+)(\sigma_{e_L^- e_L^+} + \sigma_{e_R^- e_R^+}) + (1 - P_- P_+)(\sigma_{e_L^- e_R^+} + \sigma_{e_R^- e_L^+})}, \\
1 &\geq P_- \geq 0, \quad 1 \geq P_+ \geq -1,
\end{aligned} \tag{14}$$

where the cross section in a given bin $[\theta_1, \theta_2]$ is given by $\sigma \equiv \int_{\cos \theta_1}^{\cos \theta_2} \frac{d\sigma}{d \cos \theta} d \cos \theta$. We have used $\sigma_{e_L^- e_L^+} = \sigma_{e_R^- e_R^+}$ because $\frac{d\sigma_{e_L^- e_L^+}}{d \cos \theta} - \frac{d\sigma_{e_R^- e_R^+}}{d \cos \theta} = 0$. We can also define the left-right asymmetry of the differential cross section as

$$\begin{aligned}
A_{LR}(P_-, P_+, \cos \theta) &\equiv \frac{\frac{d\sigma}{d \cos \theta}(P_{e^-} = -P_-, P_{e^+} = -P_+) - \frac{d\sigma}{d \cos \theta}(P_{e^-} = +P_-, P_{e^+} = +P_+)}{\frac{d\sigma}{d \cos \theta}(P_{e^-} = -P_-, P_{e^+} = -P_+) + \frac{d\sigma}{d \cos \theta}(P_{e^-} = +P_-, P_{e^+} = +P_+)} \\
&= \frac{(P_- + P_+) \left(\frac{d\sigma_{e_L^- e_L^+}}{d \cos \theta} - \frac{d\sigma_{e_R^- e_R^+}}{d \cos \theta} \right) + (P_- - P_+) \left(\frac{d\sigma_{e_L^- e_R^+}}{d \cos \theta} - \frac{d\sigma_{e_R^- e_L^+}}{d \cos \theta} \right)}{(1 + P_- P_+) \left(\frac{d\sigma_{e_L^- e_L^+}}{d \cos \theta} + \frac{d\sigma_{e_R^- e_R^+}}{d \cos \theta} \right) + (1 - P_- P_+) \left(\frac{d\sigma_{e_L^- e_R^+}}{d \cos \theta} + \frac{d\sigma_{e_R^- e_L^+}}{d \cos \theta} \right)} \\
&= (P_- - P_+) \cdot \frac{\Sigma_{LR-RL}}{(1 + P_- P_+) \Sigma_{LL+RR} + (1 - P_- P_+) \Sigma_{LR+RL}},
\end{aligned} \tag{15}$$

where we have used $d\sigma_{e_L^- e_L^+}/d \cos \theta = d\sigma_{e_R^- e_R^+}/d \cos \theta$ and defined

$$\begin{aligned}
\Sigma_{LL+RR} &\equiv 2s^2 |T_{LR}|^2, \\
\Sigma_{LR+RL} &\equiv u^2 (|S_{LL} + T_{LL}|^2 + |S_{RR} + T_{RR}|^2) + 2t^2 |S_{LR}|^2, \\
\Sigma_{LR-RL} &\equiv u^2 (|S_{LL} + T_{LL}|^2 - |S_{RR} + T_{RR}|^2).
\end{aligned} \tag{16}$$

In linear colliders we can measure the cross sections for $(P_{e^-}, P_{e^+}) = (P_-, P_+)$, $(P_-, -P_+)$, $(-P_-, P_+)$ and $(-P_-, -P_+)$. Combining these quantities, one can make a new observable quantity which does not depend on the value of P_{\pm} . In $e^+e^- \rightarrow e^+e^-$ scatterings we have $A_{LR}(P_-, +P_+, \cos \theta)$ and $A_{LR}(P_-, -P_+, \cos \theta)$ as independent observables and one may define the following non-trivial quantity:

$$\begin{aligned}
A_X(\cos \theta) &\equiv \frac{\Sigma_{LL+RR} - \Sigma_{LR+RL}}{\Sigma_{LL+RR} + \Sigma_{LR+RL}} \\
&= \frac{1}{P_- P_+} \cdot \frac{(P_- - P_+) A_{LR}(P_-, -P_+, \cos \theta) - (P_- + P_+) A_{LR}(P_-, +P_+, \cos \theta)}{(P_- - P_+) A_{LR}(P_-, -P_+, \cos \theta) + (P_- + P_+) A_{LR}(P_-, +P_+, \cos \theta)}.
\end{aligned} \tag{17}$$

where the second equality holds only when $P_{\pm} \neq 0$ and $|P_+| \neq |P_-|$. As is evident in the first line of (17), $A_X(\cos\theta)$ is independent of the magnitudes of polarization P_{\pm} . This quantity may be used to explore NP beyond the SM as discussed below.

Since $e^+e^- \rightarrow e^+e^-$ scattering contains t -channel processes, forward scatterings dominate. Therefore unlike the $e^+e^- \rightarrow f\bar{f}$ ($f \neq e^-$) scattering, the forward-backward asymmetry of $e^+e^- \rightarrow e^+e^-$ scattering is a less-meaningful quantity.

We note that all of the above formulas can be applied to $\ell^+\ell^- \rightarrow \ell^+\ell^-$ ($\ell = \mu, \tau$) scatterings.

4 Numerical Study

In the followings we calculate $e^+e^- \rightarrow e^+e^-$ cross sections both in the SM and GHU models, and we evaluate effects of Z' bosons in GHU models on observables given in the previous section. As benchmark points, we have chosen typical parameters of the A- and B-models in Tables 2 and 3. For experimental parameters we choose $\sqrt{s} = 250$ GeV and $L_{\text{int}} = 250 \text{ fb}^{-1}$ as typical value of linear e^+e^- colliders like ILC [61]. We also choose $L_{\text{int}} = 2 \text{ ab}^{-1}$, which will be achieved at circular e^+e^- colliders like FCC-ee [62] and CEPC [63]. For the new asymmetry $A_X(\cos\theta)$ in (17), we consider $\sqrt{s} = 3$ TeV for future linear colliders like CLIC [64]. As for the longitudinal polarization, we set the parameter ranges $-0.8 \leq P_{e^-} \leq +0.8$ and $-0.3 \leq P_{e^+} \leq 0.3$, which can be achieved at ILC [61].

In Figure 1 $e^+e^- \rightarrow e^+e^-$ differential cross sections in the SM are plotted. In the forward-scattering region ($\cos\theta > 0$), the magnitudes of cross sections of t -channel and the interference parts are much larger than those of the s -channel part.

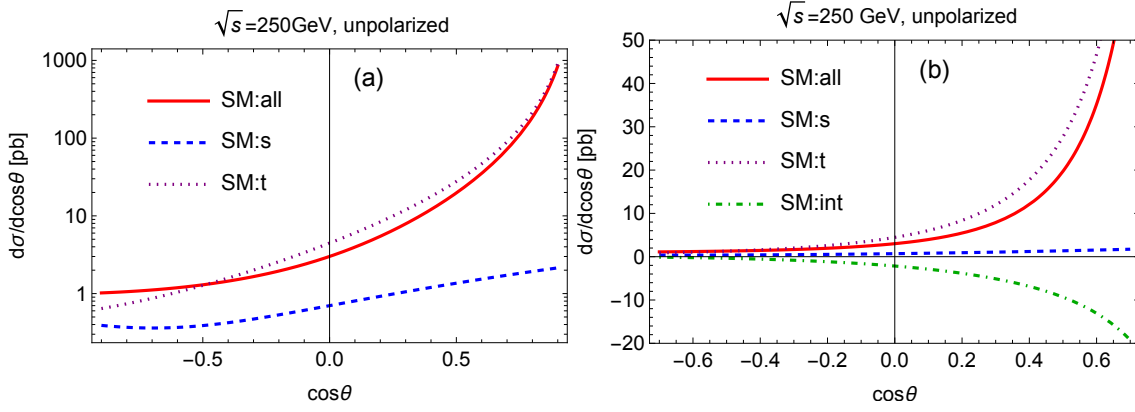


Figure 1: Differential cross sections for unpolarized e^+e^- initial states in the SM. (a) Log-scale plot with $-0.9 \leq \cos\theta \leq 0.9$. (b) Linear plot with $-0.7 \leq \cos\theta \leq 0.7$. In both plots, red-solid lines indicate the total of s -, t -channels and interferences. The s -channel and t -channel contributions are drawn as blue-dashed and purple-dotted lines, respectively. In (b), the negative contribution from interferences is plotted with the green-dashed line.

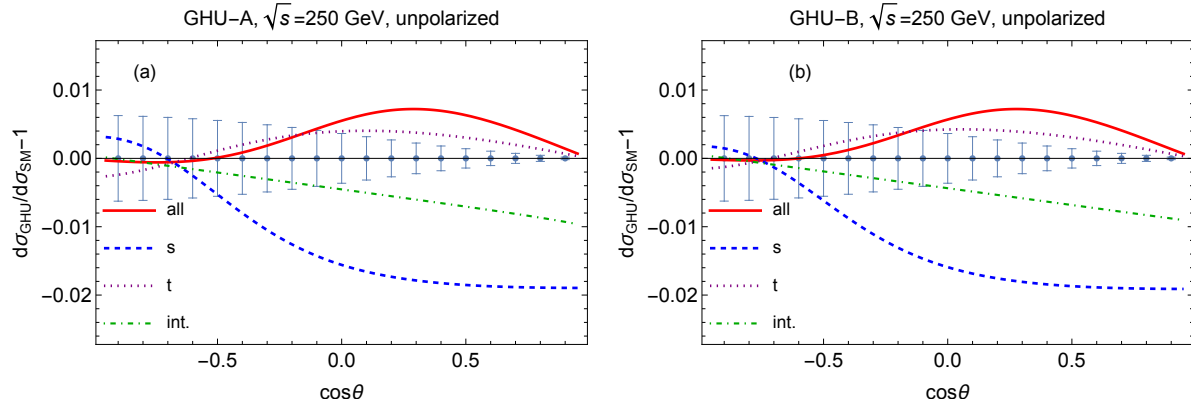


Figure 2: Deviations of differential cross sections of GHU from those in the SM, $\frac{d\sigma_{\text{GHU}}}{d\cos\theta} / \frac{d\sigma_{\text{SM}}}{d\cos\theta} - 1$, for unpolarized e^+e^- beams are plotted. The left plot is for the A-model and the right plot is for the B-model. In each plot, the red-solid curve represents the deviation of the sum of all the components of the differential cross section. Blue-dashed, purple-dotted and green dot-dashed curves correspond to the deviations of s -, t -channels and interference components of differential cross sections, respectively. Error-bars are estimated for $L_{\text{int}} = 250 \text{ fb}^{-1}$.

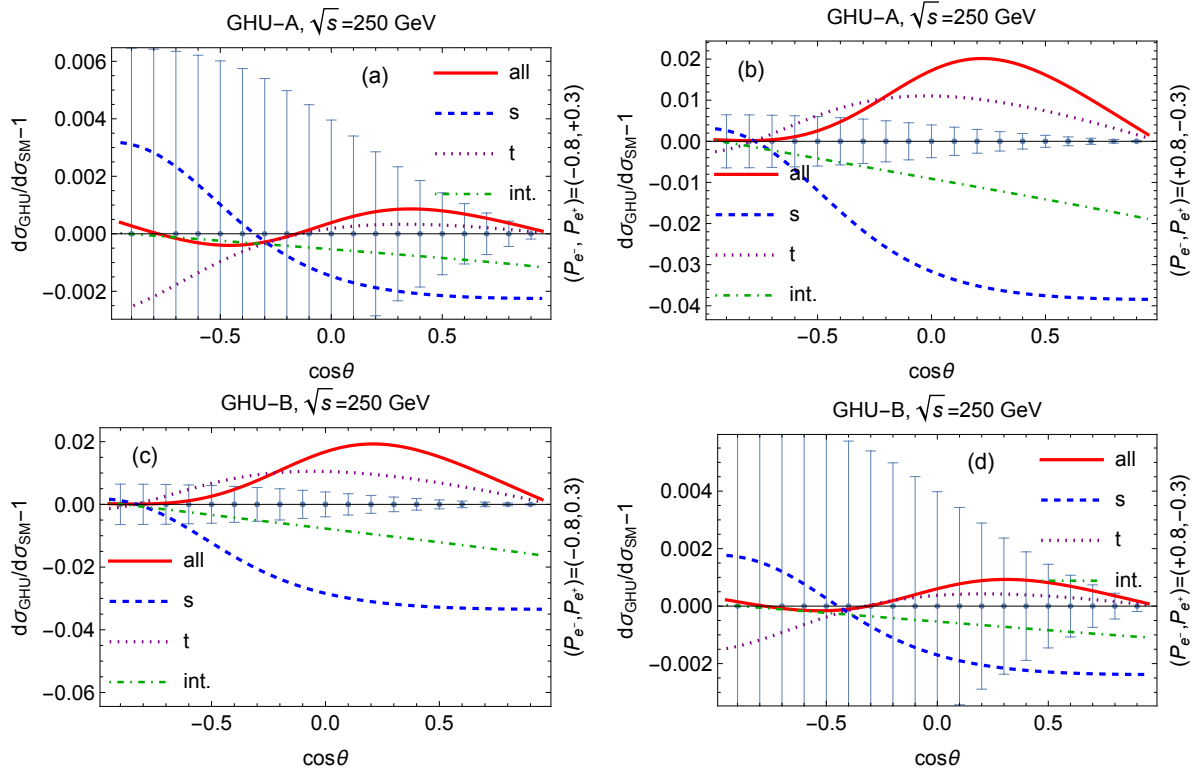


Figure 3: Deviations of differential cross sections of GHU models from the SM for polarized e^+e^- beams. GHU-A [(a) and (b)] and GHU-B [(c) and (d)]. (a) and (c) are for $(P_{e^-}, P_{e^+}) = (-0.8, +0.3)$. (b) and (d) are for $(P_{e^-}, P_{e^+}) = (+0.8, -0.3)$. Meanings of the curves and error-bars are the same as in Figure 2.

In Figures 2 and 3, the differences of differential cross sections of the GHU from the SM for unpolarized and polarized beams are plotted, respectively. In the figures, differences of s -channel, t -channel and interference contributions are also plotted. In the s -channel, the NP effects contribute destructively in the forward scattering. On the other hand, in the t -channel NP effects contribute constructively. Since the cross section is dominated by t -channel, the total of s -, t - and interference channels increases due to the NP effects.

In the A-model Z' bosons have larger couplings to right-handed electrons than to left-handed electrons. Therefore the cross section of the $e_R^- e_L^+$ initial states becomes larger than that of $e_L^- e_R^+$. On the other hand, in the B-model Z' bosons have larger couplings to left-handed electrons than to right-handed electrons, and the cross section of $e_L^- e_R^+$ initial states becomes larger.

NP effects become smaller when θ becomes smaller. The statistical uncertainty, however, also becomes small since the cross section becomes very large. Therefore deviations of the cross section relative to statistical uncertainties may become large.

For unpolarized e^+e^- beams (Figure 3), the new physics effect in both models tends to enhance the cross section at forward scattering with almost the same magnitude. In the B-model the suppression of NP effects due to larger Z' masses is compensated by larger couplings of Z' bosons than the couplings in the A-model. The enhancement of the differential cross section due to the NP effects at $\cos\theta \sim 0.3$ is around 1 %.

For polarized beams deviations can be much larger. In the A-model, electrons have large right-handed couplings to Z' bosons and for right-handed polarized beam relative deviations of the cross-section become as much as 2 % [Figure 3-(b)], whereas for right-handed beams relative deviations are around 0.1 % [Figure 3-(a)]. Contrarily, in the B-model a left-handed electron has large couplings to Z' bosons. Therefore in the B-model deviations become large for left-polarized beam [Figures 3-(c) and (d)]. In Figure 2, we have also shown statistical 1σ relative errors at $L_{\text{int}} = 250 \text{ fb}^{-1}$ for bins $[\cos\theta_0 - 0.05, \cos\theta_0 + 0.05]$ ($\cos\theta_0 = -0.90, -0.80, \dots, +0.90$) as vertical bars. In each bin, the observed number of events and statistical uncertainty are given by N and \sqrt{N} , respectively. Therefore relative error of the cross section is estimated as the inverse of the square of the number of events N .

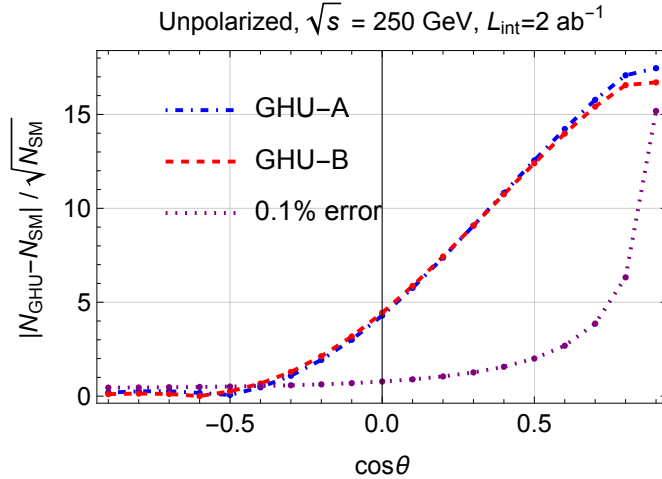


Figure 4: Estimated significances on differential cross sections of GHU models with unpolarized e^+e^- beam with the integrated luminosity $L_{\text{int}} = 2 \text{ ab}^{-1}$. A statistical significance of 0.1 % non-statistical error is plotted with a purple dot-dashed line.

In Figure 4, the statistical significances in the GHU models are plotted. An estimated significance of the deviation of the cross section in a bin is given by

$$\frac{|N_{\text{GHU}} - N_{\text{SM}}|}{N_{\text{SM}}} \bigg/ \frac{\sqrt{N_{\text{SM}}}}{N_{\text{SM}}} = \frac{|N_{\text{GHU}} - N_{\text{SM}}|}{\sqrt{N_{\text{SM}}}}, \quad (18)$$

where N_{GHU} and N_{SM} are observed numbers of events in a bin. In Figure 4, significances are larger than 5σ for $\cos\theta \gtrsim 0.1$. Significances are very large for forward scatterings, but are very small for backward scatterings. In Figure 4, relative 0.1 % errors are also shown. Errors due to the NP effects become very small and are around 0.1 % for $\cos\theta \simeq 0.9$. A similar analysis has been given in Ref. [59].

For small scattering angles θ , the scattering amplitude is dominated by t -channel contributions which are constructed with the blocks T_{LL} , T_{RR} and T_{LR} . When $|t| \simeq s\theta^2/4 \ll M_Z^2, M_{Z'}^2$, we can approximate the SM and NP contributions to the block T_{LL} in the scattering amplitude as

$$T_{LL}^{\text{NP}} \equiv \sum_{Z'} \frac{\ell_{Z'}^2}{t - M_{Z'}^2 + iM_{Z'}\Gamma_{Z'}} \simeq \sum_{Z'} \frac{\ell_{Z'}^2}{-M_{Z'}^2 + iM_{Z'}\Gamma_{Z'}}. \quad (19)$$

When $s\theta^2/4 \ll M_Z^2$, T_{LL} is dominated by the QED part $T_{LL}^{\text{QED}} \simeq -4e^2/(\theta^2 s)$ and the NP effects are estimated as

$$\frac{T_{LL}^{\text{NP}}}{T_{LL}^{\text{QED}}} \simeq \theta^2 \sum_{Z'} \frac{(\ell_{Z'}^2/4e^2)s}{M_{Z'}^2 - iM_{Z'}\Gamma_{Z'}} = \theta^2 \cdot \mathcal{O}(s/M_{Z'}^2), \quad (20)$$

and similar analysis is applied to T_{LR} and T_{RR} . Consequently, this correction arises not only in amplitudes but also in differential cross sections. For $\sqrt{s} = 250 \text{ GeV}$ and $\theta \lesssim 300 \text{ mrad}$, the QED t -channel contribution dominates and corrections due to Z' bosons are suppressed by a factor $\theta^2 s/M_{Z'}^2$. In Figure 5, deviations of differential cross sections of GHU from the SM for $\theta < 300 \text{ mrad}$ are plotted. Deviations of cross sections from the SM are proportional to the square of θ and become smaller than 0.1 % when $\theta < 250 \text{ mrad}$. The measurement of Bhabha scatterings at small scattering angle is used for the determination of the luminosity of e^+e^- collision and uncertainties of the luminosity should be smaller than 0.1 %. In GHU models the NP effects on such uncertainty are well suppressed when $\theta \lesssim 100 \text{ mrad}$. At ILC, the luminosity calorimeter in ILD (SiD) operates between 43 and 68 (40 and 90) mrad [61], where the influence of the Z' bosons is below 0.1 %.

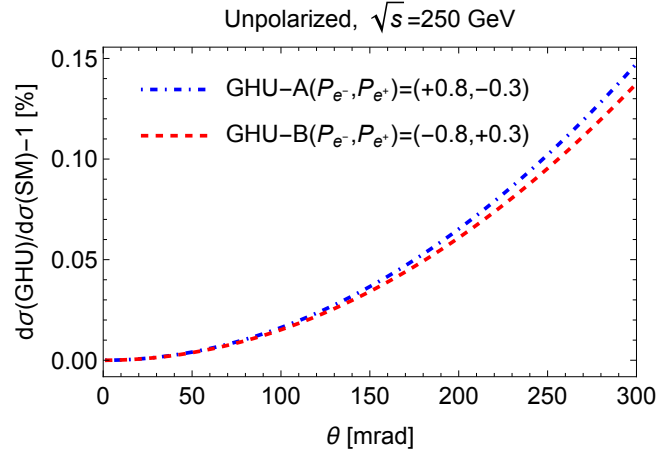


Figure 5: Deviations of differential cross sections of GHU models from the SM in the forward-scattering region ($\theta \leq 300$ mrad).

When the initial electron and positron beams are longitudinally polarized, the left-right asymmetry A_{LR} (14) can be measured. In Figure 6, the left-right asymmetries of the SM and GHU models are plotted. The measured asymmetries become larger when $|P_{e^-} - P_{e^+}|$ are larger. As seen in Figure 2, in the A-model cross section of $e_R^- e_L^+$ initial states becomes large whereas in the B-model cross section of $e_L^- e_R^+$ initial states is enhanced due to the large left-handed Z' couplings. Therefore A_{LR} of B-models are larger than the SM, whereas A_{LR} of A-models are smaller. Since the A_{LR} is proportional to $|P_{e^-} - P_{e^+}|$, the asymmetries in Figure 6-(a) are almost twice as large as in (b).

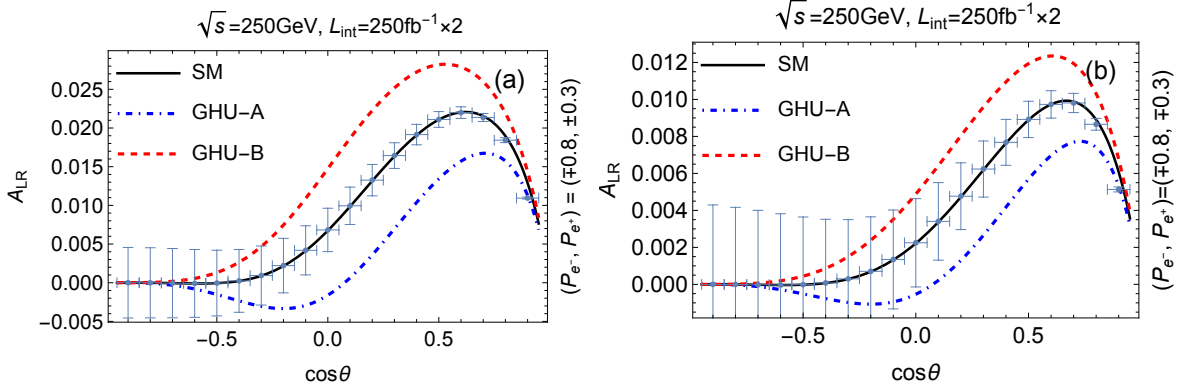


Figure 6: Left-right asymmetries. In both plots, blue-dotdashed, and red-dashed and black-solid curves correspond to the GHU-A, GHU-B and the SM, respectively. Error-bars are indicated for $L_{\text{int}} = 250 \text{ fb}^{-1}$ in each polarization. (a) Asymmetries for $(P_{e^-}, P_{e^+}) = (\mp 0.8, \pm 0.3)$. (b) Asymmetries for $(P_{e^-}, P_{e^+}) = (\mp 0.8, \mp 0.3)$.

In Figure 6, an asymmetry A_{LR} in a bin and the statistic error ΔA_{LR} are also shown. Here

$$A_{LR} = \frac{N_L - N_R}{N_L + N_R}, \quad \Delta A_{LR} = \sqrt{\frac{2(N_L^2 + N_R^2)}{(N_L + N_R)^3}} \quad (21)$$

with N_L and N_R being observed number of events for the left-handed ($P_{e^-} < 0$) and right-handed ($P_{e^-} > 0$) electron beams, respectively. For small scattering angle $\cos \theta \gtrsim 0.8$, both A_{LR}^{GHU} and A_{LR}^{SM} become close to each other.

To see how NP effects against statistical uncertainty grow for small θ , we plotted in Figure 7 the averages and statistical significances of left-right asymmetries in GHU models in each bin which are estimated as

$$\frac{A_{LR}^{\text{GHU}} - A_{LR}^{\text{SM}}}{\Delta A_{LR}}. \quad (22)$$

For the forward scattering with $\cos \theta \gtrsim 0.2$, the deviations are bigger than several times of standard deviations.

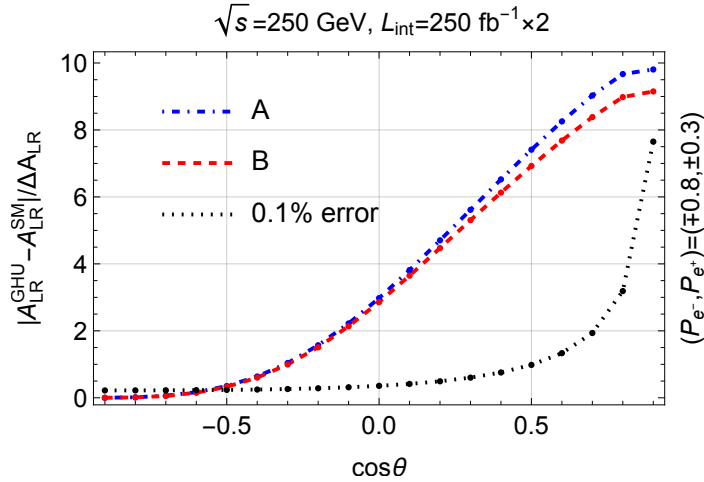


Figure 7: Estimated statistical significance on left-right asymmetries in GHU models. The blue-dotdashed, red-dashed and black-dotted lines indicate GHU-A, GHU-B and 0.1 % non-statistical errors, respectively.

In Figure 7, the significance is larger than 5σ for $\cos \theta \gtrsim 0.2$. Both models are well distinguished from the SM. Using the magnitude and sign of deviations, the A-model and B-model can be distinguished.

In Figure 8, the asymmetry A_X defined in Eq. (17) is plotted for $\sqrt{s} = 250$ GeV and $\sqrt{s} = 3$ TeV. At $\sqrt{s} = 250$ GeV, the NP effect on A_X is very small. For $\sqrt{s} = 3$ TeV, the asymmetry A_X of the SM and GHU models is clearly different and may be discriminated

experimentally. In the present analysis of NP effects, only first KK excited states of neutral bosons are taken into account. At $\sqrt{s} \sim 3$ TeV, effects of second KK modes on A_X are estimated as a few percent. These effects are much smaller than the effects of the first KK modes.

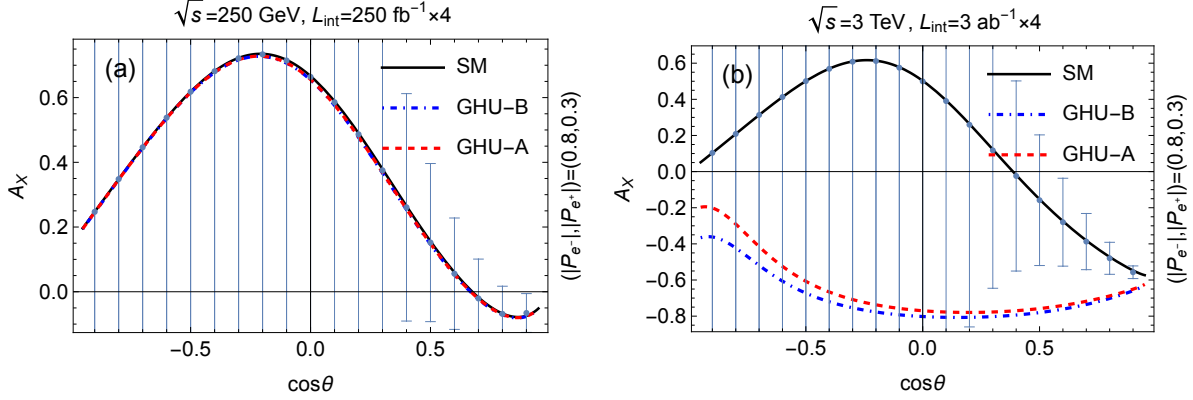


Figure 8: Plot of an asymmetry A_X in Eq. (17). The left plot (a) is for $\sqrt{s} = 250$ GeV with $L_{\text{int}} = 250 \text{ fb}^{-1}$ for each set of (P_{e-}, P_{e+}) . The right plot (b) is for $\sqrt{s} = 3$ TeV with $L_{\text{int}} = 3 \text{ ab}^{-1}$ for each set of (P_{e-}, P_{e+}) . The red-dashed, blue-dotdashed and black-solid curves correspond to the A-model, B-model and the SM, respectively. Error-bars are indicated for $L_{\text{int}} = 250 \text{ fb}^{-1}$ in (a) and $L_{\text{int}} = 3 \text{ ab}^{-1}$ in (b) in each set of (P_{e-}, P_{e+}) .

5 Summary

In this paper we examined the effects of Z' bosons in the gauge-Higgs unification (GHU) models in the $e^+e^- \rightarrow e^+e^-$ (Bhabha) scatterings. We first formulated differential cross sections in Bhabha scattering including Z' bosons. We then numerically evaluated the deviations of differential cross sections in the two $\text{SO}(5) \times \text{U}(1) \times \text{SU}(3)$ GHU models (the A- and B-models) at $\sqrt{s} = 250$ GeV. We found that at $L_{\text{int}} = 2 \text{ ab}^{-1}$ with unpolarized e^+e^- beams, the deviation due to Z' bosons in the GHU models from the SM can be clearly seen. We also found that for 80%-longitudinally polarized electron and 30%-polarized positron beams, deviations of the differential cross sections from the SM become as large as a few percent for $\cos \theta \sim 0.2$, and that the A-model and the B-model are well distinguished at more than 3σ significance at $L_{\text{int}} = 250 \text{ fb}^{-1}$. We also checked the effects of Z' bosons are negligible for the scattering angle smaller than 100 mrad at $\sqrt{s} = 250$ GeV. Therefore Bhabha scatterings at very small θ can be safely used as the measurements of the luminosity in the e^+e^- collisions. Finally we introduced the new

observable A_X . We numerically evaluated it at $\sqrt{s} = 250$ GeV and 3 TeV. Effects of the GHU models on A_X can be seen at future TeV-scale e^+e^- colliders.

In this paper the effects of Z' bosons are calculated at the Born level. Higher-order QED effects should be taken into account for more precise evaluation [65, 66].

Acknowledgements

This work was supported in part by European Regional Development Fund-Project Engineering Applications of Microworld Physics (No. CZ.02.1.01/0.0/0.0/16_019/0000766) (Y.O.), by the National Natural Science Foundation of China (Grant Nos. 11775092, 11675061, 11521064, 11435003 and 11947213) (S.F.), by the International Postdoctoral Exchange Fellowship Program (IPEFP) (S.F.), and by Japan Society for the Promotion of Science, Grants-in-Aid for Scientific Research, Nos. JP19K03873 (Y.H.) and JP18H05543 (N.Y.).

References

- [1] N. S. Manton, “*A new six-dimensional approach to the Weinberg-Salam model*”, Nucl. Phys. B **158**, 141-153 (1979).
- [2] Y. Hosotani, “*Dynamical mass generation by compact extra dimensions*”, Phys. Lett. B **126**, 309 (1983).
- [3] Y. Hosotani, “*Dynamics of nonintegrable phases and gauge symmetry breaking*”, Annals Phys. **190**, 233 (1989).
- [4] A. T. Davies and A. McLachlan, “*Gauge group breaking by Wilson loops*”, Phys. Lett. B **200**, 305-311 (1988).
- [5] A. T. Davies and A. McLachlan, “*Congruency class effects in the Hosotani model*”, Nucl. Phys. B **317**, 237 (1989).
- [6] H. Hatanaka, T. Inami and C. S. Lim, “*The gauge hierarchy problem and higher dimensional gauge theories*”, Mod. Phys. Lett. A **13**, 2601-2612 (1998), [arXiv:hep-th/9805067 [hep-th]].
- [7] H. Hatanaka, “*Matter representations and gauge symmetry breaking via compactified space*”, Prog. Theor. Phys. **102**, 407-418 (1999), [arXiv:hep-th/9905100 [hep-th]].
- [8] M. Kubo, C. S. Lim and H. Yamashita, “*The Hosotani mechanism in bulk gauge theories with an orbifold extra space S^1/Z_2* ”, Mod. Phys. Lett. A **17**, 2249-2264 (2002), [arXiv:hep-ph/0111327 [hep-ph]].

- [9] G. Burdman and Y. Nomura, “*Unification of Higgs and gauge fields in five dimensions*”, Nucl. Phys. B **656**, 3-22 (2003), [arXiv:hep-ph/0210257 [hep-ph]].
- [10] C. Csaki, C. Grojean and H. Murayama, “*Standard model Higgs from higher dimensional gauge fields*”, Phys. Rev. D **67**, 085012 (2003), [arXiv:hep-ph/0210133 [hep-ph]].
- [11] C.A. Scrucca, M. Serone, L. Silvestrini, “*Electroweak symmetry breaking and fermion masses from extra dimensions*”, Nucl. Phys. **B669**, 128 (2003).
- [12] K. Agashe, R. Contino and A. Pomarol, “*The minimal composite Higgs model*”, Nucl. Phys. B **719**, 165-187 (2005), [arXiv:hep-ph/0412089 [hep-ph]].
- [13] G. Cacciapaglia, C. Csaki, S.C. Park, “*Fully radiative electroweak symmetry breaking*”, JHEP **03**, 099 (2006), [arXiv:hep-ph/0510366 [hep-ph]].
- [14] A. D. Medina, N. R. Shah and C. E. M. Wagner, “*Gauge-Higgs unification and radiative electroweak symmetry breaking in warped extra dimensions*”, Phys. Rev. D **76**, 095010 (2007), [arXiv:0706.1281 [hep-ph]].
- [15] A. Falkowski, “*About the holographic pseudo-Goldstone boson*”, Phys. Rev. D **75**, 025017 (2007), [arXiv:hep-ph/0610336 [hep-ph]].
- [16] Y. Hosotani and Y. Sakamura, “*Anomalous Higgs couplings in the $SO(5) \times U(1)_{B-L}$ gauge-Higgs unification in warped spacetime*”, Prog. Theor. Phys. **118**, 935-968 (2007), [arXiv:hep-ph/0703212 [hep-ph]].
- [17] Y. Hosotani and Y. Kobayashi, “*Yukawa couplings and effective interactions in gauge-Higgs unification*”, Phys. Lett. B **674**, 192-196 (2009), [arXiv:0812.4782 [hep-ph]].
- [18] S. Funatsu, H. Hatanaka, Y. Hosotani, Y. Orikasa and T. Shimotani, “*Novel universality and Higgs decay $H \rightarrow \gamma\gamma$, gg in the $SO(5) \times U(1)$ gauge-Higgs unification*”, Phys. Lett. B **722**, 94-99 (2013), [arXiv:1301.1744 [hep-ph]].
- [19] S. Funatsu, H. Hatanaka, Y. Hosotani, Y. Orikasa and T. Shimotani, “*LHC signals of the $SO(5) \times U(1)$ gauge-Higgs unification*”, Phys. Rev. D **89**, no.9, 095019 (2014), [arXiv:1404.2748 [hep-ph]].
- [20] S. Funatsu, H. Hatanaka, Y. Hosotani and Y. Orikasa, “*Collider signals of W' and Z' bosons in the gauge-Higgs unification*”, Phys. Rev. D **95**, no.3, 035032 (2017), [arXiv:1612.03378 [hep-ph]].
- [21] S. Funatsu, H. Hatanaka, Y. Hosotani and Y. Orikasa, “*Distinct signals of the gauge-Higgs unification in e^+e^- collider experiments*”, Phys. Lett. B **775**, 297-302 (2017), [arXiv:1705.05282 [hep-ph]].

- [22] H. Hatanaka, “*Thermal phase transition in the $SO(5) \times U(1)$ gauge-Higgs unification with 126GeV Higgs*”, [arXiv:1304.5104 [hep-ph]].
- [23] S. Funatsu, H. Hatanaka, Y. Hosotani, Y. Orikasa and N. Yamatsu, “*GUT inspired $SO(5) \times U(1) \times SU(3)$ gauge-Higgs unification*”, Phys. Rev. D **99**, no. 9, 095010 (2019), [arXiv:1902.01603 [hep-ph]].
- [24] S. Funatsu, H. Hatanaka, Y. Hosotani, Y. Orikasa and N. Yamatsu, “*CKM matrix and FCNC suppression in $SO(5) \times U(1) \times SU(3)$ gauge-Higgs unification*”, Phys. Rev. D **101**, no.5, 055016 (2020), [arXiv:1909.00190 [hep-ph]].
- [25] S. Funatsu, H. Hatanaka, Y. Hosotani, Y. Orikasa and N. Yamatsu, “*Fermion pair production at e^-e^+ linear collider experiments in GUT inspired gauge-Higgs unification*”, Phys. Rev. D **102**, no.1, 015029 (2020), [arXiv:2006.02157 [hep-ph]].
- [26] S. Funatsu, “*Forward-backward asymmetry in the gauge-Higgs unification at the International Linear Collider*”, Eur. Phys. J. **C79**, 854 (2019), [arXiv:1905.10007 [hep-ph]].
- [27] S. Funatsu, H. Hatanaka, Y. Hosotani, Y. Orikasa and N. Yamatsu, “*Electroweak and left-right phase transitions in $SO(5) \times U(1) \times SU(3)$ gauge-Higgs unification*”, Phys. Rev. D **104**, no.11, 115018 (2021), [arXiv:2104.02870 [hep-ph]].
- [28] S. Funatsu, H. Hatanaka, Y. Hosotani, Y. Orikasa and N. Yamatsu, “*Signals of W' and Z' bosons at the LHC in the $SU(3) \times SO(5) \times U(1)$ gauge-Higgs unification*”, Phys. Rev. D **105** 055015, [arXiv:2111.05624 [hep-ph]].
- [29] J. Yoon and M. E. Peskin, “*Competing forces in five-dimensional fermion condensation*”, Phys. Rev. D **96**, no.11, 115030 (2017), [arXiv:1709.07909 [hep-ph]].
- [30] J. Yoon and M.E. Peskin, “*Fermion pair production in $SO(5) \times U(1)$ gauge-Higgs unification models*”, arXiv:1811.07877 [hep-ph].
- [31] J. Yoon and M.E. Peskin, “*Dissection of an $SO(5) \times U(1)$ gauge-Higgs unification model*”, Phys. Rev. D **100**, no.1, 015001 (2019), [arXiv:1810.12352 [hep-ph]].
- [32] N. Kurahashi, C. S. Lim and K. Tanabe, “*Anomalous Higgs interactions in dimensional deconstruction*”, PTEP **2014**, no.12, 123B04 (2014), [arXiv:1406.2549 [hep-ph]].
- [33] Y. Matsumoto and Y. Sakamura, “*Yukawa couplings in 6D gauge-Higgs unification on T^2/Z_N with magnetic fluxes*”, PTEP **2016**, no.5, 053B06 (2016), [arXiv:1602.01994 [hep-ph]].
- [34] K. Hasegawa and C. S. Lim, “*Majorana neutrino masses in the scenario of gauge-Higgs unification*”, PTEP **2018**, no.7, 073B01 (2018), [arXiv:1804.04270 [hep-ph]].

- [35] M. Kakizaki and S. Suzuki, “*Higgs potential in gauge-Higgs unification with a flat extra dimension*”, Phys. Lett. B **822**, 136637 (2021), [arXiv:2107.13445 [hep-ph]].
- [36] C.S. Lim and N. Maru, “*Towards a realistic grand gauge-Higgs unification*”, Phys. Lett. **B653**, 320 (2007), [arXiv:0706.1397 [hep-ph]].
- [37] Y. Hosotani and N. Yamatsu, “*Gauge–Higgs grand unification*”, PTEP **2015**, 111B01 (2015), [arXiv:1504.03817 [hep-ph]].
- [38] A. Furui, Y. Hosotani and N. Yamatsu, “*Toward realistic gauge-Higgs grand unification*”, PTEP **2016**, no.9, 093B01 (2016), [arXiv:1606.07222 [hep-ph]].
- [39] Y. Hosotani and N. Yamatsu, “*Electroweak symmetry breaking and mass spectra in six-dimensional gauge–Higgs grand unification*”, PTEP **2018**, no.2, 023B05 (2018), [arXiv:1710.04811 [hep-ph]].
- [40] C. Englert, D. J. Miller and D. D. Smaranda, “*Phenomenology of GUT-inspired gauge-Higgs unification*”, Phys. Lett. B **802**, 135261 (2020), [arXiv:1911.05527 [hep-ph]].
- [41] C. Englert, D. J. Miller and D. D. Smaranda, “*The Weinberg angle and 5D RGE effects in a SO(11) GUT theory*”, Phys. Lett. B **807**, 135548 (2020), [arXiv:2003.05743 [hep-ph]].
- [42] M. Kakizaki, S. Kanemura, H. Taniguchi and T. Yamashita, “*Higgs sector as a probe of supersymmetric grand unification with the Hosotani mechanism*”, Phys. Rev. D **89**, no.7, 075013 (2014), [arXiv:1312.7575 [hep-ph]].
- [43] K. Kojima, K. Takenaga and T. Yamashita, “*The standard model gauge symmetry from higher-rank unified groups in grand gauge-Higgs unification models*”, JHEP **06**, 018 (2017), [arXiv:1704.04840 [hep-ph]].
- [44] N. Maru and Y. Yatagai, “*Improving fermion mass hierarchy in grand gauge-Higgs unification with localized gauge kinetic terms*”, Eur. Phys. J. C **80**, no.10, 933 (2020), [arXiv:1911.03465 [hep-ph]].
- [45] A. Angelescu, A. Bally, S. Blasi and F. Goertz, “*Minimal SU(6) gauge-Higgs grand unification*”, Phys. Rev. D **105**, no.3, 035026 (2022), [arXiv:2104.07366 [hep-ph]].
- [46] L. Randall and R. Sundrum, “*A large mass hierarchy from a small extra dimension*”, Phys. Rev. Lett. **83**, 3370-3373 (1999), [arXiv:hep-ph/9905221 [hep-ph]].
- [47] T. Barklow, K. Fujii, S. Jung, R. Karl, J. List, T. Ogawa, M. E. Peskin and J. Tian, “*Improved formalism for precision Higgs coupling fits*”, Phys. Rev. D **97**, no.5, 053003 (2018), [arXiv:1708.08912 [hep-ph]].
- [48] E. Senaha, “*Symmetry restoration and breaking at finite temperature: An introductory review*”, Symmetry **12**, no.5, 733 (2020).

- [49] S. Bilokin, R. Pöschl and F. Richard, “*Measurement of b quark EW couplings at ILC*”, arXiv:1709.04289 [hep-ex].
- [50] A. Irles, R. Pöschl, F. Richard and H. Yamamoto, “*Complementarity between ILC250 and ILC-GigaZ*”, Linear Collider Community Meeting, arXiv:1905.00220 [hep-ex].
- [51] A. Irles, R. Pöschl and F. Richard, “*Production and measurement of $e^+e^- \rightarrow c\bar{c}$ signatures at the 250 GeV ILC*”, LCWS 2019, arXiv:2002.05805 [hep-ex].
- [52] S. Schael *et al.* [ALEPH and DELPHI and L3 and OPAL and SLD Collaborations and LEP Electroweak Working Group and SLD Electroweak Group and SLD Heavy Flavour Group], “*Precision electroweak measurements on the Z resonance*”, Phys. Rept. **427**, 257 (2006), [hep-ex/0509008].
- [53] S. Schael *et al.* [ALEPH, DELPHI, L3, OPAL and LEP Electroweak], “*Electroweak measurements in electron-positron collisions at W -boson-pair energies at LEP*”, Phys. Rept. **532**, 119-244 (2013), [arXiv:1302.3415 [hep-ex]].
- [54] G. Moortgat-Pick *et al.*, “*The Role of polarized positrons and electrons in revealing fundamental interactions at the linear collider*”, Phys. Rept. **460**, 131 (2008), [hep-ph/0507011].
- [55] A. Arbuzov, S. Bondarenko and L. Kalinovskaya, “*Asymmetries in processes of electron-positron annihilation*”, Symmetry **12**, no.7, 1132 (2020), [arXiv:2007.03908 [hep-ph]].
- [56] K. Abe *et al.* [SLD Collaboration], “*Polarized Bhabha scattering a precision measurement of the electron neutral current couplings*”, Phys. Rev. Lett. **74**, 2880 (1995), [hep-ex/9410009].
- [57] K. Abe *et al.* [SLD Collaboration], “*Precise measurement of the left-right cross-section asymmetry in Z boson production by e^+e^- collisions*”, Phys. Rev. Lett. **73**, 25-29 (1994), [arXiv:hep-ex/9404001 [hep-ex]].
- [58] K. Abe *et al.* [SLD Collaboration], “*An improved measurement of the left-right Z^0 cross-section asymmetry*”, Phys. Rev. Lett. **78**, 2075-2079 (1997), [arXiv:hep-ex/9611011 [hep-ex]].
- [59] F. Richard, “*Bhabha scattering at ILC250*”, arXiv:1804.02846 [hep-ex].
- [60] A. Das, P. S. B. Dev, Y. Hosotani and S. Mandal, “*Probing the minimal $U(1)_X$ model at future electron-positron colliders via the fermion pair-production channel*”, [arXiv:2104.10902 [hep-ph]].

- [61] K. Fujii et al., “*Physics case for the 250 GeV stage of the International Linear Collider*”, arXiv:1710.07621 [hep-ex]; H. Baer, et.al., “*The International Linear Collider Technical Design Report - Volume 2: Physics*”, [arXiv:1306.6352 [hep-ph]]; T. Behnke, et.al., “*The International Linear Collider Technical Design Report - Volume 4: Detectors*”, [arXiv:1306.6329 [physics.ins-det]].
- [62] A. Blondel and P. Janot, “*FCC-ee overview: new opportunities create new challenges*”, Eur. Phys. J. Plus **137**, no.1, 92 (2022), [arXiv:2106.13885 [hep-ex]].
- [63] J. B. Guimarães da Costa et al. [CEPC Study Group], “*CEPC conceptual design report: Volume 2 - Physics & Detector*”, [arXiv:1811.10545 [hep-ex]].
- [64] L. Luice, M. Akiya, S. Marcel and W. Harry, “*Physics and Detectors at CLIC: CLIC Conceptual Design Report*”, CERN-2012-003, [arXiv:1202.5940 [physics.ins-det]].
- [65] D. Y. Bardin, W. Hollik and T. Riemann, “*Bhabha scattering with higher order weak loop corrections*”, Z. Phys. C **49**, 485 (1991).
- [66] D. Bardin, Y. Dydyshka, L. Kalinovskaya, L. Rumyantsev, A. Arbuzov, R. Sadykov and S. Bondarenko, “*One-loop electroweak radiative corrections to polarized Bhabha scattering*”, Phys. Rev. D **98**, no. 1, 013001 (2018), [arXiv:1801.00125 [hep-ph]].